and the Early Solar System, J. F. Kerridge and M. S. Matthews, Eds. (Univ. of Arizona Press, Tucson, 1988), pp. 35–67.

3. J. F. Bell, D. R. Davis, W. K. Hartmann, M. J. Gaffey, in *Asteroids II*, R. P. Binzel, T. Gehrels, M. S. Matthews, Eds. (Univ. of Arizona Press, Tucson, 1989), pp. 921–945.
4. For example, B. Zellner, D. J. Tholen, E. F. Tedesco, *Icarus* **61**, 355 (1985); F. Vilas and L. A. McFadden, *ibid.* **100**, 85 (1993); J. X. Luu and D. C. Jewitt, *Astron. J.* **99**, 1985 (1990).
5. R. P. Binzel and S. Xu, in preparation.
6. ———, *Science* **260**, 186 (1993). The instrumentation provides a spectral dispersion of 10 Å per pixel.
7. M. F. Skrutskie, M. R. Meyer, R. Coutu, in preparation.
8. These data were calibrated with the use of infrared standard stars from a list compiled at the United Kingdom Infrared Telescope [M. M. Casali, *JCMT UKIRT Newsl.* **4**, 33 (1992)] transformed into the California Institute of Technology (CIT) photometric system [J. Elias *et al.*, *Astron J.* **87**, 1029 (1982)]. All infrared data in this report are quoted in the CIT system, which matches the natural system of the NICMASS instrument within the errors of measurement.
9. The MDM Observatory is located on Kitt Peak near Tucson, AZ, and McD Observatory is located on Mount Locke near Fort Davis, TX. Simultaneous observations from these observatories were performed on 7 March 1993 UT. The J and H filter measurements were made at Kitt Peak over the interval of 6:04 to 6:50 UT, while the R filter measurements were made in Texas during 6:13 to 6:56 UT. The observations were coordinated from the first author's kitchen table in Lexington, MA, with a notebook computer and modem connection to the Internet communications network.
10. All references to the R filter in this report correspond to the Kron-Cousins system [A. W. J. Cousins, *Mem. R. Astron. Soc.* **81**, 25 (1976)].
11. L. A. McFadden, M. J. Gaffey, T. B. McCord, *Science* **229**, 160 (1985).
12. M. J. Gaffey, J. F. Bell, D. P. Cruikshank, in (*3*), pp. 98–127.
13. M. J. Gaffey, *J. Geophys. Res.* **81**, 905 (1976).
14. Transition metals and their cations, for example, Fe^{2+}, give rise to most geologically diagnostic absorptions (*12*). Independent physical processes create the absorptions at short and long wavelengths such that their characteristics are not highly correlated. Below ~0.5 μm, absorptions are caused by charge transfers between electron orbital shells within many silicate and oxide minerals. Beyond 1 μm, absorptions are caused by field splitting arising from the crystal structure of the specific minerals present. In general, the long wavelength absorptions are much more diagnostic of the mineralogy.
15. G. W. Wetherill, *Philos. Trans. R. Soc. London Ser. A* **323**, 323 (1987).
16. J. Wisdom, *Icarus* **56**, 51 (1983); *Nature* **315**, 731 (1985).
17. Starting with the measured magnitude in the R filter (Table 2), we assume solar-like V-R filter colors to estimate a V filter magnitude of 18.07. At the time of observation, the asteroid was 3.257 AU from the sun, 2.322 AU from the Earth, and at a solar phase angle of 6.92°. We assume the same value for the phase coefficient, $G = 0.12$, as is tabulated for 1862 Apollo [E. F. Tedesco, in (*3*), pp. 1090–1138]. We also assume the tabulated albedo for Apollo, $\rho_V = 0.21$ [L. A. McFadden, D. J. Tholen, G. J. Veeder, in (*3*), pp. 442–467]. From these geometric and assumed values, we derive an absolute magnitude $H = 13.13$ and diameter of 7 km using the relations presented by E. Bowell and colleagues [in (*3*), pp. 524–556].
18. The age of 951 Gaspra, the 1991 flyby target for the Galileo spacecraft, is estimated to be ~3 × 10^8 years, as predicted by N. Namiki and R. P. Binzel [*Geophys. Res. Lett.* **18**, 1155 (1991)].
19. Specifically, we refer to the "S(IV)" class of asteroids defined by M. J. Gaffey and co-workers (*Icarus*, in press).
20. H. Campins, G. H. Rieke, M. J. Lebofsky, *Astron. J.* **90**, 896 (1985); M. S. Bessel and M. J. Brett, *Publ. Astron. Soc. Pac.* **100**, 1134 (1988).
21. D. P. Cruikshank and W. K. Hartmann, *Science* **223**, 281 (1984).
22. J. F. Bell, P. D. Owensby, B. R. Hawke, M. J. Gaffey, *Lunar Planet. Sci.* **19**, 57 (1988).
23. A. Milani and Z. Knezevic, *Icarus* **98**, 211 (1992).
24. Data reported here were obtained in part at the MDM Observatory. We thank B. Barr (MDM Observatory) and J. Martin (McD Observatory) for exceptional technical support that allowed these observations to be made, L. Hillenbrand for assistance with the NICMASS observations, and two anonymous reviewers for their helpful suggestions. Supported by National Aeronautics and Space Administration grants NAGW 1450 (R.P.B.) and NAGW 1477 (McD Observatory) and by the Astrophysical Research Consortium through its role in the infrared component of this work through the Detector Development Consortium.

29 June 1993; accepted 5 October 1993

SSZ-26 and SSZ-33: Two Molecular Sieves with Intersecting 10- and 12-Ring Pores

Raul F. Lobo, Ming Pan, Ignatius Chan, Hong-Xin Li,
Ronald C. Medrud, Stacey I. Zones, Peter A. Crozier,
Mark E. Davis*

The framework structures of two closely related molecular sieves, SSZ-26 and SSZ-33, are described. These materials possess a previously missing but desired structural feature in a group of industrially significant zeolites. They contain a three-dimensional pore system that provides access to the crystal interior through both 10- and 12-rings. This property is a consequence of the organic structure–directing agents used in the synthesis of these materials. These materials are examples of the purposeful design of a micropore architecture. Both SSZ-26 and SSZ-33 contain the 4=4−1 building unit that had been previously found only in natural zeolites.

Inorganic molecular sieves, such as zeolites, are extensively used in catalytic and separation processes, especially in the petrochemical and refining industries (*1*, *2*). New large-pore materials, those with pores bounded by rings composed of 12 tetrahedral (T) atoms (such as Si, Al, and B) with open-pore diameters of ~7 Å (*3*, *4*), can be used for controlled shape-selective catalysis of molecules with relatively complex architectures. Large-pore materials with intersecting channels also have increased resistance to fouling and enhanced intracrystalline diffusion properties over materials with unidimensional channels; however, only a few zeolites are known with pores that are both large and intersecting. Zeolites Y and beta have intersecting 12-ring pores and have extensive application in refinery processes, as does zeolite ZSM-5, which has intersecting 10-ring (medium) pores. Additionally, as environmental factors play more significant roles in the design of new process chemistries, zeolite solid acids—because of their ease of handling and disposal—are receiving close attention as possible substitutes of the currently used liquid acids.

A molecular sieve with intersecting 10- and 12-ring pores is likely to offer a combination of reaction activity, selectivity, and stability not found in any other material (*4*). Only recently, a zeolite with intersecting 10- and 12-ring pores was found in the rare mineral boggsite (*5*). Additionally, the synthetic material NU-87 (*6*) has a 10- and 12-ring pore system, but access to the crystal interior can only be achieved through the 10-ring pores. Thus, this type of zeolite is of interest for catalytic applications in the petrochemical industry but, until now, was only available in the minute quantities of boggsite, too low for even laboratory-scale evaluation.

Several factors prompted us to study the structures of the synthetic zeolites SSZ-26 and the related SSZ-33. First, preliminary sorption experiments indicated that these materials had a multidimensional pore system with at least one of the pores being a 12-ring. Second, the structure-directing agents used for the synthesis of both materials were carefully chosen such that they would form a multidimensional pore system (*7*). Additionally, the concepts of structure-direction could be tested if a close relation between the structure-directing agent and the pore geometry could be found.

SSZ-26 and SSZ-33 (*7–9*) are synthesized

R. F. Lobo, H.-X. Li, M. E. Davis, Chemical Engineering, California Institute of Technology, Pasadena, CA 91125.
M. Pan and P. A. Crozier, Center for Solid State Science, Arizona State University, Tempe, AZ 85287–1704.
I. Chan, R. C. Medrud, S. I. Zones, Chevron Research and Technology Company, Richmond, CA 94802–0627.

*To whom correspondence should be addressed.

under hydrothermal conditions with the use of organic structure–directing agents **I** and **II**, respectively (see below). SSZ-26 is typically synthesized with a SiO_2/Al_2O_3 ratio of 20 to 50, whereas SSZ-33 is normally crystallized with a SiO_2/B_2O_3 ratio of ~30. Similarities in their x-ray powder diffraction (XRD) patterns, sorption data, and catalytic properties suggested that these two materials have related crystal structures.

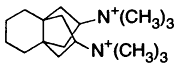

I

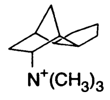

II

The synchrotron XRD pattern of SSZ-33 showed a combination of sharp and broad features that suggested the presence of stacking disorder in the structure. The sharp reflections were indexed on an orthorhombic unit cell with dimensions a = 13.26 Å, b = 12.33 Å, and c = 21.08 Å. Except for the (0 1 0) reflection, the remaining reflections were of the form $(h\ 3n\ 1)$, $n = 0, 1, 2$, which is indicative of shears associated with faulting of ±1/3b. This kind of faulting is also present in zeolite beta (*10*) and NU-86 (*11*).

Single-crystal electron diffraction (ED) patterns along one zone axis contained sharp diffraction intensities for every third column of reflections and streakings for the remaining reflections. Such characteristic intensity distribution is a manifestation of a layered structure with heavy stacking faults as a result of the presence of both ABABAB . . . and ABCABC. . . stacking sequences. The lateral displacement for successive layers is one-third of the intralayer spacing. This observation is consistent with the XRD data. The ED data obtained by systematically tilting the crystal showed that the crystallites had an orthorhombic structure with lattice parameters similar to those obtained by XRD.

A low-dose high resolution electron micrograph (HREM) recorded in the [100] projection (Fig. 1A) shows direct evidence for the two different stacking sequences deduced from the XRD and ED patterns (*12*). Careful analysis of the image intensities indicates that the main pores (large bright dots) are 10-rings, and the secondary features (small bright dots) represent eight 5- and two 6-rings in the structure (*13, 14*).

Two related structures consistent with the unit cell dimensions and physical properties of SSZ-33 were constructed. The structures can be thought of as being formed by sheets related by translation of [1/2, ±1/3, 1/2] (with the basis vectors of the orthorhombic unit cell described above). If the sheets are arranged with alternate translations (ABABAB . . . stacking sequence), a structure with orthorhombic symmetry is formed. By analogy to the nomenclature developed for zeolite beta by Newsam *et al.* (*10*), this structure is called polymorph A and belongs to the space group *Pmna* (no. 53) with unit cell dimensions a = 13.26 Å, b = 12.33 Å, and c = 21.08 Å (Fig. 2, A

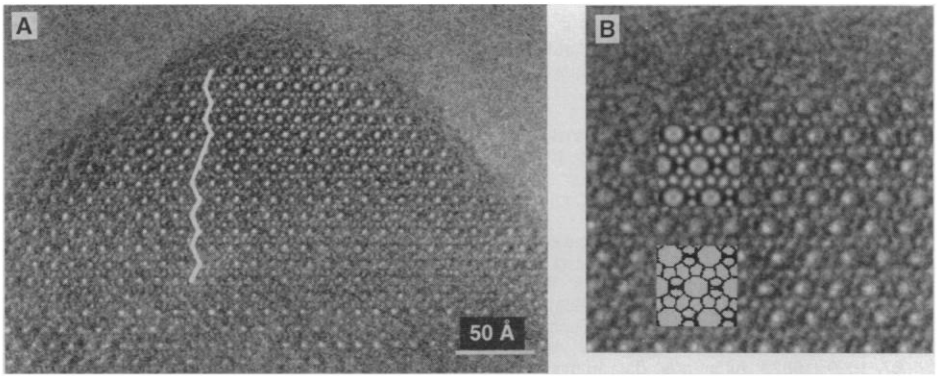

Fig. 1. (**A**) Low-dose HREM image of a small crystal of SSZ-33 viewed along the [100] direction. Large bright dots in the image show the location of the 10-ring pores in this projection. Intergrowth of both polymorphs A (zig-zag line) and B (straight line) are indicated. This image was recorded digitally with a slow-scan CCD (charge-coupled device) camera. (**B**) An enlarged HREM image showing the structure details of polymorph A. The simulated image and structure projection are top and bottom insets.

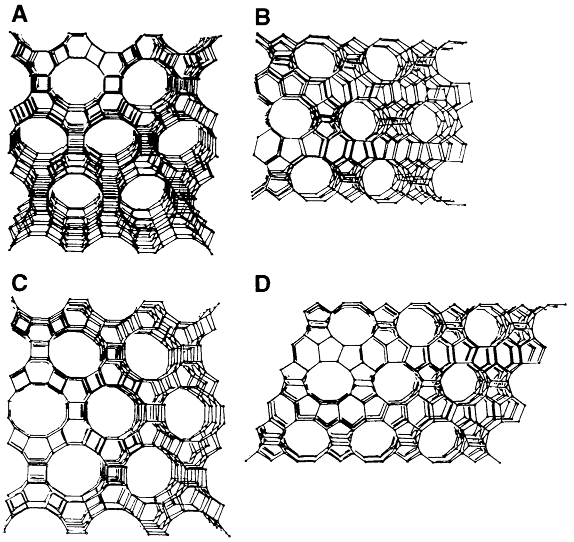

Fig. 2. Framework structure of polymorph A viewed along the 12-ring pores (**A**) and along the 10-ring pores (**B**), and framework structure of polymorph B viewed along the 12-ring pores (**C**) and the 10-ring pores (**D**). The view along the 10-ring pores of polymorph A (B) shows the effect the shears of ±1/3b in alternate sequence (ABAB. . .stacking sequence). Similarly, the view along the 10-ring pores of polymorph B (D) shows the effect of consecutive shears of 1/3b in one direction (ABCABC. . .stacking sequence).

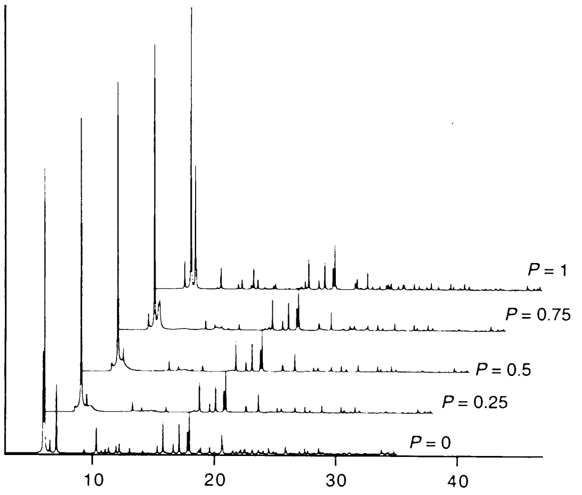

Fig. 3. Effect of faulting on the XRD pattern. The faulting probability P is defined as the probability of reversal in the direction of stacking. A value of $P = 0$ forms the end member polymorph B where all the layers are stacked in the same direction with respect to the previous one, and a value of $P = 1$ gives the XRD pattern of polymorph A, where the direction of stacking is changed in each layer. The simulations were carried out with synchrotron radiation with a wavelength λ of 1.19505 Å.

and B). If the sheets are arranged with translations always in the same direction (ABCABC. . .stacking sequence), a monoclinic polymorph B is formed with space group *B*2/*m* (no. 12) and unit cell dimensions a = 13.26 Å, b = 12.33 Å, c = 22.62 Å, and α = 68.7° (Fig. 2, C and D). Both polymorphs have a three-dimensional pore system formed by intersecting 10- and 12-ring pores. The atomic coordinates of the oxygen and T atoms were optimized with distance least squares refinement (Tables 1 and 2) [DLS-76, (*15, 16*)], and HREM images of each polymorph were simulated and compared with the experimental data.

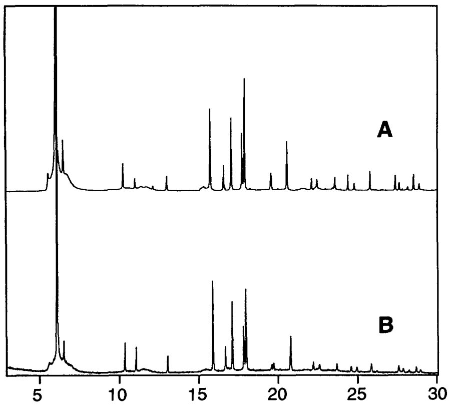

Fig. 4. Comparison of the calculated synchrotron XRD pattern of SSZ-33 (**A**) and the experimental XRD pattern (**B**) of the intergrowth with a fault probability P = 0.3 (λ = 1.19505 Å).

Table 1. Distance least squares optimized atomic coordinates for polymorph A [space group *Pmna* (no. 53), a = 13.26 Å, b = 12.33 Å, and c = 21.08 Å].

Atom*	x	y	z
T1	0.111	0.208	0.074
T2	0.114	0.158	0.927
T3	0.211	0.030	0.150
T4	0.113	0.463	0.072
T5	0.198	0.359	0.849
T6	0.112	0.960	0.271
T7	0.116	0.711	0.278
O1	0.192	0.148	0.117
O2	0.123	0.168	0.002
O3	0.129	0.336	0.078
O4	0.000	0.180	0.099
O5	0.150	0.269	0.895
O6	0.184	0.061	0.903
O7	0.000	0.135	0.908
O8	0.311	0.017	0.181
O9	0.117	0.018	0.204
O10	0.000	0.494	0.091
O11	0.134	0.500	0.000
O12	0.190	0.525	0.118
O13	0.314	0.330	0.836
O14	0.137	0.361	0.783
O15	0.000	0.969	0.299
O16	0.141	0.835	0.263
O17	0.000	0.700	0.298

*T, tetrahedral atoms.

Very good agreement is observed between the model for polymorph A and the experimental image (Fig. 1B). The synchrotron XRD, ED, and the HREM (Fig. 1A) indicate, however, that SSZ-33 is an intergrowth of these two structures. Simulated XRD patterns incorporating the disorder [using DIFFaX (*17*)] are illustrated in Fig. 3. Comparison of the simulated with the experimental XRD patterns indicates that SSZ-33 is an intergrowth of polymorph A and polymorph B with a predominance of polymorph B and a fault probability close to 30% (Fig. 4).

For the zeolite SSZ-26, the isomorphous substitution of Al for B increases the unit cell dimensions because of the longer Al–O bond (1.72 Å) compared with the B–O bond (1.48 Å). On the basis of the indexing of the sharp reflections of the XRD pattern of SSZ-26, the unit cell dimensions of polymorph A are a = 13.43 Å, b = 12.40 Å, and c = 21.23 Å, and the unit cell dimensions of polymorph B are a = 13.43 Å, b = 12.40 Å, c = 22.78 Å, and α = 68.8°. Comparison of the simulated and experimental XRD patterns indicated that there is also a predominance of polymorph B in SSZ-26, but the faulting probability is close to 15% (Fig. 5). Complete details of the structure solution of SSZ-33 and SSZ-26 will be given elsewhere (*18*).

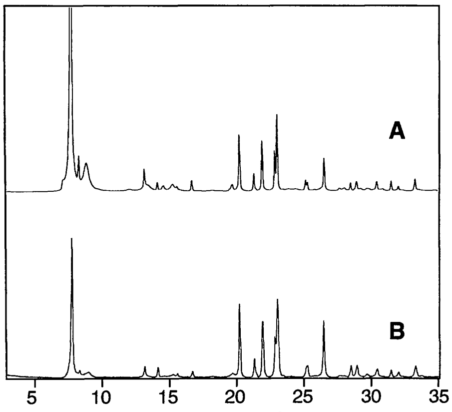

Fig. 5. Comparison of the calculated XRD pattern of SSZ-26 (**A**) and the experimental XRD pattern (**B**) of the intergrowth with a fault probability P = 0.15 (λ = 1.5406 Å).

Table 2. Distance least squares optimized atomic coordinates for polymorph B [space group *B*2/*m* (no. 12), a = 13.26 Å, b = 12.33 Å, c = 22.62 Å, and α = 68.7°].

Atom*	x	y	z
T1	0.118	0.500	0.068
T2	0.199	0.267	0.147
T3	0.111	0.751	0.072
T4	0.115	0.101	0.274
T5	0.115	0.849	0.279
T6	0.114	0.123	0.074
T7	0.200	0.872	0.153
O1	0.000	0.472	0.077
O2	0.139	0.626	0.071
O3	0.180	0.404	0.123
O4	0.153	0.500	0.000
O5	0.127	0.203	0.206
O6	0.174	0.221	0.091
O7	0.314	0.239	0.168
O8	0.000	0.748	0.100
O9	0.114	0.845	0.001
O10	0.191	0.786	0.115
O11	0.000	0.094	0.296
O12	0.147	0.980	0.269
O13	0.186	0.127	0.324
O14	0.127	0.827	0.214
O15	0.000	0.828	0.302
O16	0.000	0.117	0.099
O17	0.167	0.000	0.109

*T, tetrahedral atoms.

Unlike zeolite beta, which crystallizes with a stacking probability of 50% whether synthesized as borosilicate, aluminosilicate, or gallosilicate (*10*), the existence of SSZ-26 and SSZ-33 suggests that materials with a fault probability from 0 to 100% may be prepared.

These materials fill a long-existing gap in the type of molecular sieve materials available. SSZ-26 and SSZ-33 are molecular sieves whose multidimensional pore systems have been formed by the purposeful design of their organic structure-directing agents (*7*). Experimentally, it has been observed that the structure-directing agent is intact inside the pores of SSZ-26 (*7*) and that the number of molecules per unit cell is the same as the number of pore intersections. Additionally, molecular simulations indicate that the structure-directing agent of SSZ-26 conforms to the geometry of the intersection of the 10- and 12-ring pores (*18*) as originally proposed (*19*). The geometry of the organic molecule is the most important factor in obtaining a pore system intermediate in size to the zeolites ZSM-5 and beta. In addition to the large pore system, the frameworks of SSZ-26 and SSZ-33 are high-silica molecular sieves that contain the 4=4−1 secondary building unit (*3*). This unit has only been found in natural zeolites before the synthesis of SSZ-26. Numerous natural zeolites such as heulandite, stilbite, and boggsite have the 4=4−1 building unit among their structural building blocks and have not been readily synthesized under hydrothermal conditions in the laboratory. The synthesis of SSZ-26 and SSZ-33 suggests that other large-pore materials that include this unit may be synthesized.

REFERENCES AND NOTES

1. J. M. Newsam, in *Solid State Chemistry: Compounds*, A. K. Cheetham and P. Day, Eds. (Oxford Univ. Press, New York, 1992), pp. 234–280.
2. M. E. Davis, *Chem. Ind. London* 4, 137 (1992).
3. W. M. Meier and D. H. Olson, *Atlas of Zeolite Structure Types* (Butterworths-Heineman, Stoneham, MA, 1992).
4. M. E. Davis and R. F. Lobo, *Chem. Mater.* 4, 756 (1992).

5. J. J. Pluth and J. V. Smith, *Am. Mineral.* **75**, 501 (1990).
6. M. D. Shannon *et al.*, *Nature* **353**, 417 (1991).
7. S. I. Zones, M. M. Olmstead, D. S. Santilli, *J. Am. Chem. Soc.* **114**, 4195 (1992).
8. S. I. Zones *et al.*, U.S. Patent 4 910 006 (1990).
9. S. I. Zones, U.S. Patent 4 963 337 (1990).
10. J. M. Newsam, M. M. J. Treacy, W. T. Koetsier, C. B. de Gruyter, *Proc. R. Soc. London Ser. A* **420**, 375 (1988).
11. M. D. Shannon, in *Proceedings of the 9th International Zeolites Conference*, R. von Ballmoos, J. B. Higgins, M. M. Treacy, Eds. (Butterworth-Heinemann, Stoneham, MA, 1993), vol. 1, pp. 389–398.
12. M. Pan and P. A. Crozier, *Ultramicroscopy* **48**, 322 (1993).
13. ———, *ibid.*, in press.
14. M. Pan *et al.*, in preparation.
15. C. Baerlocher, A. Hepp, W. M. Meier, *DLS-76* (Institut fur Kristallographie, ETH, Zürich, 1976). The weighted agreement values for polymorph A were $R = 0.0013$, $\sigma = 0.007$ and for polymorph B were $R = 0.001$, $\sigma = 0.005$. The unit cell dimensions were held constant during the optimization by using the values obtained from the indexing of the synchrotron XRD pattern of SSZ-33. $\langle T–O \rangle = 1.60$ Å [assuming Si:B = 15, Si–O = 1.605 Å (*10*), and B–O = 1.48 Å].
16. The distance least squares refinement and the simulation of the XRD patterns of polymorph A and polymorph B were carried out with the program CERIUS 3.1 from Molecular Simulations.
17. M. M. J. Treacy, M. W. Deem, J. M. Newsam, *Proc. R. Soc. London Ser. A* **433**, 499 (1991). The simulations were carried out with the atom positions obtained from the distance least squares optimization of polymorph A. Silicon was used in all T atom positions.
18. R. F. Lobo *et al.*, in preparation.
19. S. I. Zones and D. S. Santilli, in *Proceedings of the 9th International Zeolites Conference*, R. von Ballmoos, J. B. Higgins, M. M. Treacy, Eds. (Butterworth-Heinemann, Stoneham, MA, 1993), vol. 1, pp. 171–179.
20. We are grateful to Chevron Research and Technology Company for financial support. We thank W. P. Schaefer and R. E. Marsh for comments on the manuscript. We acknowledge D. E. Cox for assistance in collecting the synchrotron data. The XRD data were collected at X7A beam line, National Synchrotron Light Source, Brookhaven National Laboratory, which is supported by the Department of Energy, Division of Material Sciences and Division of Chemical Sciences. We also acknowledge the assistance of G. Zhang and G. Mondo, from Chevron Research and Technology Company, in collecting the synchrotron data. M.P. and P.A.C. were supported by the HREM Industrial Associates Program at Arizona State University. HREM work was done at the Center for HREM at Arizona State University supported by NSF grant DMR9115680.

7 July 1993; accepted 7 October 1993

Engineered Biosynthesis of Novel Polyketides

Robert McDaniel, Susanne Ebert-Khosla, David A. Hopwood, Chaitan Khosla*

Polyketide synthases (PKSs) are multifunctional enzymes that catalyze the biosynthesis of a huge variety of carbon chains differing in their length and patterns of functionality and cyclization. Many polyketides are valuable therapeutic agents. A *Streptomyces* host-vector system has been developed for efficient construction and expression of recombinant PKSs. Using this expression system, several novel compounds have been synthesized in vivo in significant quantities. Characterization of these metabolites has provided new insights into key features of actinomycete aromatic PKS specificity. Thus, carbon chain length is dictated, at least in part, by a protein that appears to be distinctive to this family of PKSs, whereas the acyl carrier proteins of different PKSs can be interchanged without affecting product structure. A given ketoreductase can recognize and reduce polyketide chains of different length; this ketoreduction always occurs at the C-9 position. The regiospecificity of the first cyclization of the nascent polyketide chain is either determined by the ketoreductase, or the chain-extending enzymes themselves. However, the regiospecificity of the second cyclization is determined by a distinct cyclase, which can discriminate between substrates of different chain lengths.

Polyketides occur in most groups of organisms and are especially abundant in a class of mycelial bacteria, the actinomycetes. They are an extremely rich source of bioactive molecules, including antibiotics (such as tetracyclines and erythromycin), anticancer agents (daunomycin), immunosuppressants (FK506 and rapamycin), and veterinary products (monensin and avermectin). Like the related fatty-acid synthases (FASs), the polyketide synthases (PKSs) are multifunctional enzymes that catalyze repeated decarboxylative condensations between coenzyme A (CoA) thioesters (usually acetyl, propionyl, malonyl, or methylmalonyl). After each condensation, FASs typically catalyze a complete reductive cycle comprising a ketoreduction, dehydration, and enoylreduction on the β-keto group of the growing carbon chain, whereas PKSs omit this cycle or curtail it after some or even all condensation steps. After the carbon chain has grown to a length characteristic of each specific product, it is released from the synthase by thiolysis or acyltransfer (*1*). It is the controlled variation in chain length, choice of chain-building units, and the reductive cycle, genetically programmed into each PKS, that leads to the huge variation among naturally occurring polyketides (*2*).

Although the rules of this programming have hitherto been obscure, current genetics-led research is beginning to clarify them. Cloning and sequencing of PKS genes has suggested two entirely different programming strategies. One is represented by the PKSs for macrolides such as erythromycin, which consist of several large multifunctional proteins carrying, between them, a set of separate active sites for every individual step of carbon-chain assembly and modification (*3*). There is thus a one-to-one correlation between the number and clustering of active sites in the primary sequence of the PKS and the structural features of the polyketide backbone. The second class of PKSs, represented by the synthases for aromatic compounds, has a single set of iteratively used active sites (*4–6*). It follows that the programming mechanism for this class of PKS is not apparent from the number and arrangement of active sites.

We report the development of a *Streptomyces* host-vector system that allows the facile construction of minimal sets of genes for natural or hybrid combinations of PKS components (or mutants thereof) and the expression of the gene sets to produce novel polyketide products. The advantages of the system are that the genes are expressed in a quasi-natural manner to produce significant quantities of product at an appropriate stage of the growth cycle, and that the products themselves undergo a minimum of post-PKS reactions. Thus, determination of product structure gives direct insights into aspects of PKS programming. The results reported here include the discovery that a specific component of the PKS is responsible, at least in part, for determining carbon chain length, that either the ketoreductase or the chain-extending enzymes play a key role in dictating the regiospecificity of the first cyclization of the nascent carbon chain, and that further cyclization is determined by the specificity of a cyclase. Five new compounds generated by this system are reported here and elsewhere (*7*). The system holds great promise for the generation of a wide range of potentially useful metabolites.

Streptomyces coelicolor A3(2), a model actinomycete with well-developed genetics (*8*), produces the blue-pigmented polyketide, actinorhodin (1) (Fig. 1). The biosynthetic pathway has been partially elucidated (*9–11*), and the *act* gene cluster has

---

R. McDaniel, S. Ebert-Khosla, C. Khosla, Department of Chemical Engineering, Stanford University, Stanford, CA 94305–5025.
D. A. Hopwood, Department of Genetics, John Innes Institute, John Innes Centre, Norwich NR4 7UH, United Kingdom.

*To whom correspondence should be addressed.